

Unveiling the Interplay among End Group, Molecular Packing, Doping Level, and Charge Transport in N-Doped Small-Molecule Organic Semiconductors

Gao-Yang Ge, Jia-Tong Li, Juan-Rong Wang, Miao Xiong, Xue Dong, Zu-Jian Li, Jiu-Long Li, Xiao-Yu Cao, Ting Lei,* and Jin-Liang Wang*

Doped small molecules with high electrical conductivity are desired because they typically show a larger Seebeck coefficient and lower thermal conductivity than their polymer counterparts. However, compared with conjugated polymers, only a few small molecules can show high electrical conductivities. In this study, three n-type small-molecule organic semiconductors with different end functional groups are synthesized to explore the reasons for the low electrical conductivity issue in n-doped small-molecule semiconductors. Charge carrier mobility and doping level are usually considered as two major parameters for achieving high electrical conductivity. TDPP-Th1C with high electron mobility of $0.77 \text{ cm}^2 \text{ V}^{-1} \text{ s}^{-1}$ and high electron affinity, which can be easily n-doped; however, it only displays an electrical conductivity $\approx 10^{-3} \text{ S cm}^{-1}$. To explore the reasons, the single crystal structure of TDPP-Th1C and the grazing incidence wide-angle X-ray scattering of its n-doped films are carefully analyzed. TDPP-Th1C with a 1D column packing is disclosed and easily distorted by the enthetic n-dopants, which damages the charge transport pathways, and thereby results in low electrical conductivity. The results suggests that only high intrinsic charge carrier mobility and high doping level cannot guarantee high electrical conductivity, and keeping good charge transport pathways after doping is also critical.

1. Introduction

Organic thermoelectric (OTE) materials have attracted considerable attention because of their low toxicity, being light-

weight, good solution processability, and lower thermal conductivity (κ) compared to inorganic thermoelectric materials.^[1–5] The thermoelectric property of an OTE material can be evaluated by the figure of merit, (ZT):

$$ZT = S^2 \sigma T / \kappa \quad (1)$$

where T , S , and σ are the absolute temperature, Seebeck coefficient, and electrical conductivity, respectively. Besides, power factor ($PF = S^2 \sigma$) is also commonly used to characterize the performance of an OTE material due to the usually low thermal conductivities in doped organic semiconductors. P-type OTE materials, such as poly(3,4-ethylene dioxythiophene) (PEDOT), have exhibited high electrical conductivity over 1000 S cm^{-1} with ZT over 0.4. This ZT value is approaching that of inorganic materials, especially for low-temperature thermoelectric applications.^[6,7] Compared with the fast advance of p-type OTE materials, the performance of n-type OTE materials still lags behind, largely due to their low doped electrical conductivity.^[8–12]

To address this challenge, significant efforts have been devoted to the development of new n-type conjugated polymers

G.-Y. Ge, Z.-J. Li, J.-L. Wang
Key Laboratory of Cluster Science of Ministry of Education
Beijing Key Laboratory of Photoelectronic/Electrophotonic Conversion Materials
School of Chemistry and Chemical Engineering
Beijing Institute of Technology
Beijing 100081, China
E-mail: jinliwang@bit.edu.cn
J.-T. Li, J.-R. Wang, J.-L. Li, T. Lei
Key Laboratory of Polymer Chemistry and Physics of Ministry of Education
School of Materials Science and Engineering
Peking University
Beijing 100871, China
E-mail: tinglei@pku.edu.cn

M. Xiong
Key Laboratory of Polymer Chemistry and Physics of Ministry of Education
College of Chemistry and Molecular Engineering
Peking University
Beijing 100871, China
X. Dong, X.-Y. Cao
State Key Laboratory of Physical Chemistry of Solid Surfaces
iChEM and College of Chemistry and Chemical Engineering
Xiamen University
Xiamen 361005, China

 The ORCID identification number(s) for the author(s) of this article can be found under <https://doi.org/10.1002/adfm.202108289>.

DOI: 10.1002/adfm.202108289

and new n-doping processes.^[13–27] Recently, high electrical conductivity of over 90 S cm⁻¹ has been achieved in a n-doped strong electron-deficient conjugated polymer.^[28] Although the high electrical conductivity has been obtained, the *PF* and *ZT* value (76 μW m⁻¹ K⁻² and 0.06, respectively) of the doped conjugated polymer are usually low because of its low Seebeck coefficient (approximately -91 μV K⁻¹), which may originate from the low charge carrier mobility and large structural and energetic disorders.^[9,29]

Small molecules have precise structures, negligible batch-to-batch variation, better crystallinity, ordered molecular packing, and usually higher charge carrier mobilities.^[30–32] To date, only a few small molecules are employed for n-type doping.^[33–36] Di and co-workers found that with the high electron mobility of 0.89 cm² V⁻¹ s⁻¹, aromatic-dicyanovinyl-dipyrrolo[3,4-c]pyrrole-1,4-diylidene-bis(thieno[3,2-b]thiophene (A-DCV-DPPTT) showed a high Seebeck coefficient of -699 μV K⁻¹ and a *PF* of 236 μW m⁻¹ K⁻² with the *ZT* value up to 0.26 after doped with a widely used dopant *N*-DMBI.^[37] Later, Koster and co-workers reported a fullerene derivative with ethylene glycol polar side chain, exhibiting a Seebeck coefficient of -235 μV K⁻¹ and *PF* of 46 μW m⁻¹ K⁻² after doped with 5 wt% *N*-DMBI. However, because of its low κ (0.064 W m⁻¹ K⁻¹), a *ZT* value of 0.34 was obtained, which is currently the highest value for n-type OTE materials.^[38] These studies suggest that small-molecule organic semiconductors could show higher Seebeck coefficients and lower thermal conductivities than conjugated polymers, making them more promising for TE applications. Compared with the great efforts that have been devoted to conjugated polymers, only a few small-molecule OTE materials are explored and used, largely due to their poor mechanical flexibility, less morphological or thermal stability, and low electrical conductivities after doping,^[39–41] even though small molecules have shown

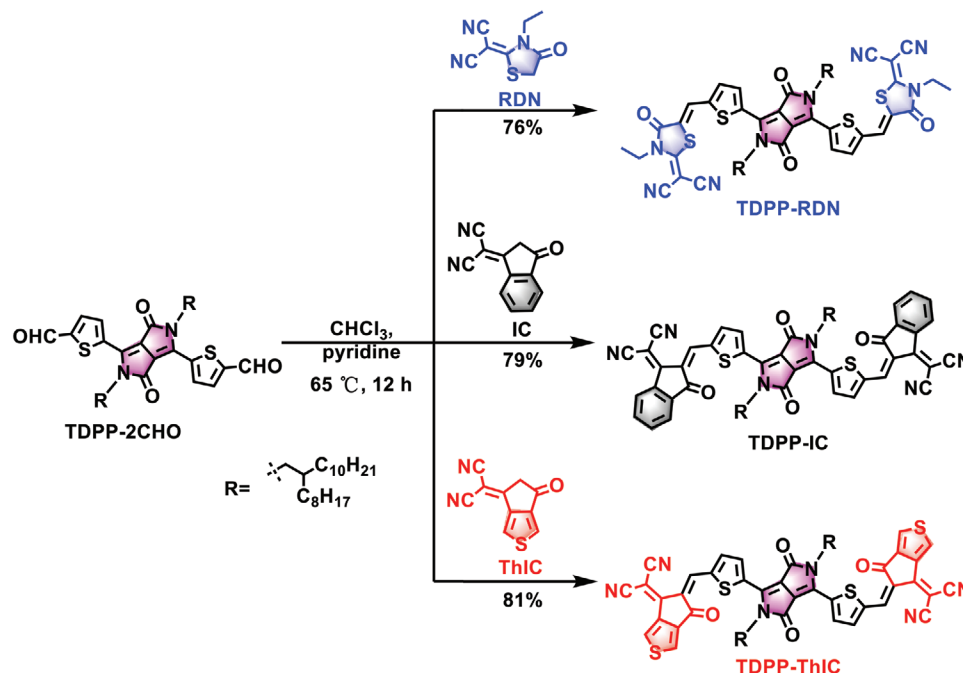
high charge carrier mobilities and can be readily n-doped. However, the reasons for the low electrical conductivity after doping are still obscure.

Here we synthesized three small molecules, TDPP-RDN, TDPP-IC, and TDPP-ThIC, to explore the limitations of using small molecules in OTE applications (Scheme 1). The three molecules have the same dithienyl diketopyrropyrrole (TDPP) core but with different electron-withdrawing end functional groups. TDPP-RDN, TDPP-IC, and TDPP-ThIC show gradually the deeper lowest unoccupied molecular orbital (LUMO) energy levels. Among them, TDPP-ThIC shows an outstanding electron mobility of up to 0.77 cm² V⁻¹ s⁻¹, higher than those of TDPP-RDN and TDPP-IC (0.07 and 0.18 cm² V⁻¹ s⁻¹, respectively). Benefitting from its high electron affinity, TDPP-ThIC can be effectively doped by *N*-DMBI. However, its electrical conductivity is only ≈10⁻³ S cm⁻¹. To explore the reasons, single crystal structure and the grazing incidence wide-angle X-ray scattering (GIWAXS) were used. We find that the molecular packing of pristine TDPP-ThIC film is easily distorted by the n-dopants, which damages the charge transport pathways, lowers the film crystallinity, and thereby results in low electrical conductivity.

2. Results and Discussion

2.1. Synthesis and Structure Characterization

The synthetic routes of TDPP-RDN, TDPP-IC, and TDPP-ThIC are displayed in Scheme 1. We choose diketopyrropyrrole (DPP) as the building block because of its good planarity, strong intermolecular interaction, and potentially high charge carrier mobility.^[42–45] Dicyanomethylene-3-ethylrhodanine (RDN) and



Scheme 1. Synthetic routes of TDPP-RDN, TDPP-IC, and TDPP-ThIC.

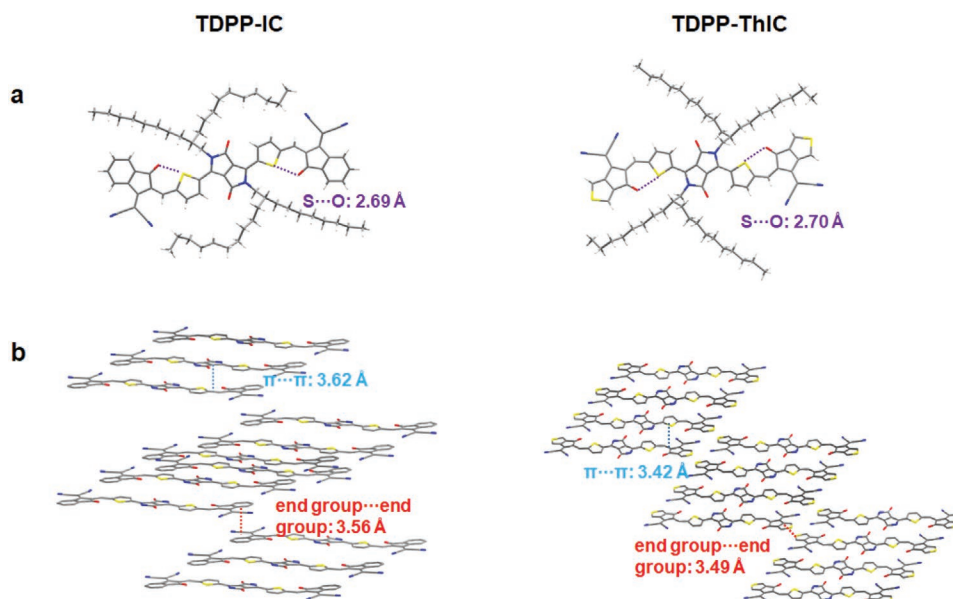


Figure 1. a) The crystallographic structures and b) the molecular packings of TDPP-IC and TDPP-ThIC. The red-, yellow-, blue-, and gray-colored atoms represent O, S, N, and C, respectively. The long alkyl chains in molecular packing are omitted for clarity.

3-(dicyanomethylidene)-indan-1-one (IC) are chosen as end functional groups because of their strong electron-withdrawing ability.^[46–49] Particularly, thiophene-fused IC (ThIC) not only has a strong electron-withdrawing ability but could also provide better intermolecular interactions because of its potentially heteroatomic non-covalent interactions.^[50–52] After Knoevenagel condensation reaction between TDPP-2CHO^[53] and RDN, IC, or ThIC, respectively, three DPP-based small molecules were obtained with the high yield of 76% for TDPP-RDN, 79% for TDPP-IC, and 81% for TDPP-ThIC. The structures of TDPP-RDN, TDPP-IC, and TDPP-ThIC were well characterized by ¹H NMR, ¹³C NMR, and high-resolution mass spectrometry (HRMS). Their thermal properties were investigated by thermogravimetric analysis (TGA) and differential scanning calorimeter (DSC). As shown in Figure S1, Supporting Information, all the molecules show good thermal stability with the decomposition temperatures over 320 °C. Differential scanning calorimeter (DSC) measurement shows that the melting/crystallization temperatures (T_m/T_c) are 212/193 °C for TDPP-RDN, 287/258 °C for TDPP-IC, and 290/265 °C for TDPP-ThIC, respectively, suggesting their different intermolecular interactions caused by different end functional groups. Usually the higher the melting points, the stronger the intermolecular interactions.

The single crystal structures of TDPP-IC and TDPP-ThIC were obtained by slowly diffusing ethanol to their chlorobenzene (CB) solutions, and efforts to obtain the single crystal structure of TDPP-RDN were unsuccessful. The crystallographic structures are shown in **Figure 1**, and the crystallographic data are summarized in Table S1, Supporting Information. Both molecules show the similar triclinic crystal structures, and the S...O distances (2.69 Å for TDPP-IC and 2.69 Å TDPP-ThIC) are less than the sum of their van der Waals radii of S and O (3.25 Å) (Figure 1a), indicating the existence of intramolecular non-covalent interactions, which provide both molecules with

highly planar and conformation-locked backbones.^[54] Besides, TDPP-IC and TDPP-ThIC both show 1D column packings with the intracolumn π - π stacking distances of 3.62 Å for TDPP-IC and 3.42 Å for TDPP-ThIC. The intercolumn interactions are formed through the π - π stacking of the end functional groups, and the π - π stacking distances between two columns are 3.56 Å for TDPP-IC and 3.49 Å for TDPP-ThIC. All the results imply that TDPP-ThIC has a relatively closer π - π stacking distance than TDPP-IC, and the intracolumn interactions seem stronger than intercolumn interactions.

2.2. Photophysical and Electrochemical Properties

All the molecules show typical two-band absorptions with Band II (350–550 nm) and Band I (550–1000 nm) (**Figure 2a,b**). The strong absorption band, Band I, can be attributed to the intramolecular charge transfer (ICT) absorption according to literature.^[55] All the molecules show two vibrational peaks in Band I, namely 0-0 and 0-1. Compared to the solution absorption spectra, film spectra show obvious red-shift, suggesting strong intermolecular interactions in solid state. Interestingly, the relative intensities of the two vibrational peaks vary: the 0-0 vibrational peaks are stronger in solution; while the 0-1 vibrational peaks are stronger in solid state. This phenomenon suggests a typical H-like aggregate in solid state,^[56,57] which is consistent with the columnar molecular packing observed in the single crystal structures.

The energy levels of the molecules were evaluated by cyclic voltammetry (CV). Three molecules showed reversible reduction behaviors (Figure S2, Supporting Information). Their highest occupied molecular orbital (HOMO)/LUMO energy levels were estimated to be -5.39/-3.85 eV for TDPP-RDN, -5.58/-3.99 eV for TDPP-IC, and -5.65/-4.05 eV for TDPP-ThIC, respectively (Figure 2c and **Table 1**). The gradually lower

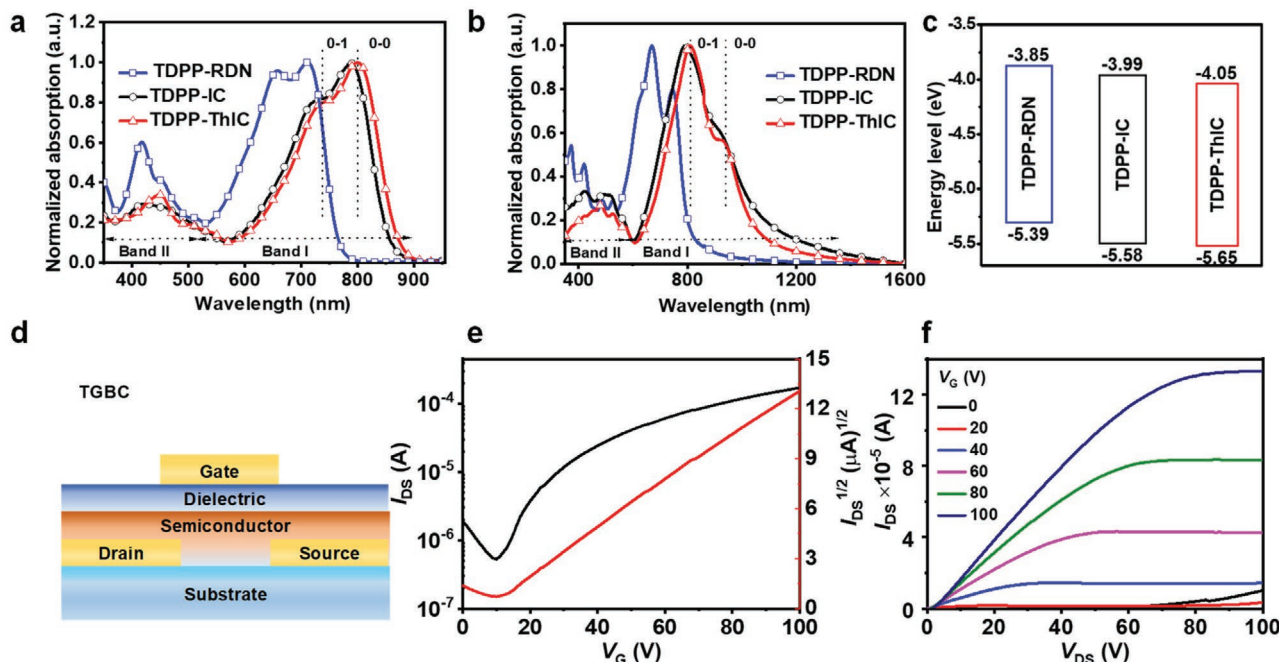


Figure 2. Normalized absorption spectra of TDPP-RDN, TDPP-IC, and TDPP-ThIC a) in diluted CB solution (10^{-5} M) and b) in thin films. c) Energy level diagrams of the three molecules. d) The configuration of the top-gate and bottom-contact (TGBC) FET device. e) Typical transfer and f) output characteristics of a TDPP-ThIC FET device ($W/L = 20$, $C_i = 3.7$ nF cm^{-2}).

LUMO energy levels imply stronger electron-withdrawing ability from RDN, IC to ThIC. The molecular properties were also explored using density functional theory (DFT) calculations (Figure S3, Supporting Information). All the molecules show planar backbones, and their HOMOs mainly distribute on the TDPP cores, while their LUMOs delocalize over the entire molecules. The calculated HOMO/LUMO energy levels are $-5.61/-3.83$ eV for TDPP-RDN, $-5.56/-3.92$ eV for TDPP-IC, and $-5.61/-4.00$ eV for TDPP-ThIC, respectively, which are consistent with the tendency of cyclic voltammetric results.

2.3. Charge Transport and Solid-State Microstructures of the Pristine Films

The charge transport properties of these molecules were evaluated by top-gate and bottom-contact (TGBC) field-effect transistor (FET). The devices were prepared by spin-coating the molecules' solutions (5 mg mL^{-1} in CB) onto a SiO_2 substrate and annealing at 150 °C, followed by a commercially available CYTOP dielectric layer deposition. Typical transfer and output characteristics of the molecules are shown in Figure 2 and

Figure S4, Supporting Information. All the molecules show typical n-type charge transport behaviors because of their low-lying LUMO energy levels. Among all the molecules, TDPP-ThIC exhibits high electron mobilities (μ_e) of up to 0.77 cm^2 V^{-1} s^{-1} , which are much higher than those of TDPP-RDN and TDPP-IC (0.07 and 0.18 cm^2 V^{-1} s^{-1} , respectively) (Table 1). Considering that three molecules have very similar backbones and identical side chains, the significant difference of electron mobility is largely due to their different end functional groups that may lead to different intermolecular interactions. The contact resistances of TDPP-IC and TDPP-ThIC films were also measured via the modified transmission-line method (TLM).^[58,59] From Figure S5, Supporting Information, TDPP-IC devices show a higher contact resistance than TDPP-ThIC devices, which might explain the observed lower electron mobility for TDPP-IC films. This might be due to the higher LUMO energy level of TDPP-IC.

The molecular packings and film microstructures of the pristine films were investigated by GIWAXS and atomic force microscopy (AFM) (Figure 3). The corresponding q_{xy} orientation line-cuts and q_z orientation line-cuts are shown in Figure S6, Supporting Information. We found that the thin film molecular

Table 1. Optical, electrochemical, and charge transport properties of TDPP-RDN, TDPP-IC, and TDPP-ThIC.

Materials	$\lambda_{\text{sol}}^{\text{a}}$ [nm]	$\lambda_{\text{fil}}^{\text{b}}$ [nm]	$E_{\text{HOMO}}^{\text{c}}$ [eV]	$E_{\text{LUMO}}^{\text{c}}$ [eV]	E_g^{c} [eV]	$E_{\text{HOMO}}^{\text{d}}$ [eV]	$E_{\text{LUMO}}^{\text{d}}$ [eV]	$\mu_{e,\text{max}}^{\text{e}}$ (cm^2 V^{-1} s^{-1})
TDPP-RDN	657, 710	670, 744	-5.39	-3.85	1.54	-5.61	-3.83	0.07 (0.06 ± 0.01)
TDPP-IC	730, 787	792, 915	-5.58	-3.99	1.59	-5.56	-3.92	0.18 (0.16 ± 0.02)
TDPP-ThIC	740, 800	809, 924	-5.65	-4.05	1.60	-5.61	-4.00	0.77 (0.59 ± 0.17)

^a) In CB solution; ^b) In thin film; ^c) Obtained by CV measurement; ^d) Estimated from DFT calculations; ^e) The data in brackets are the average mobilities with standard deviation obtained from at least six FET devices.

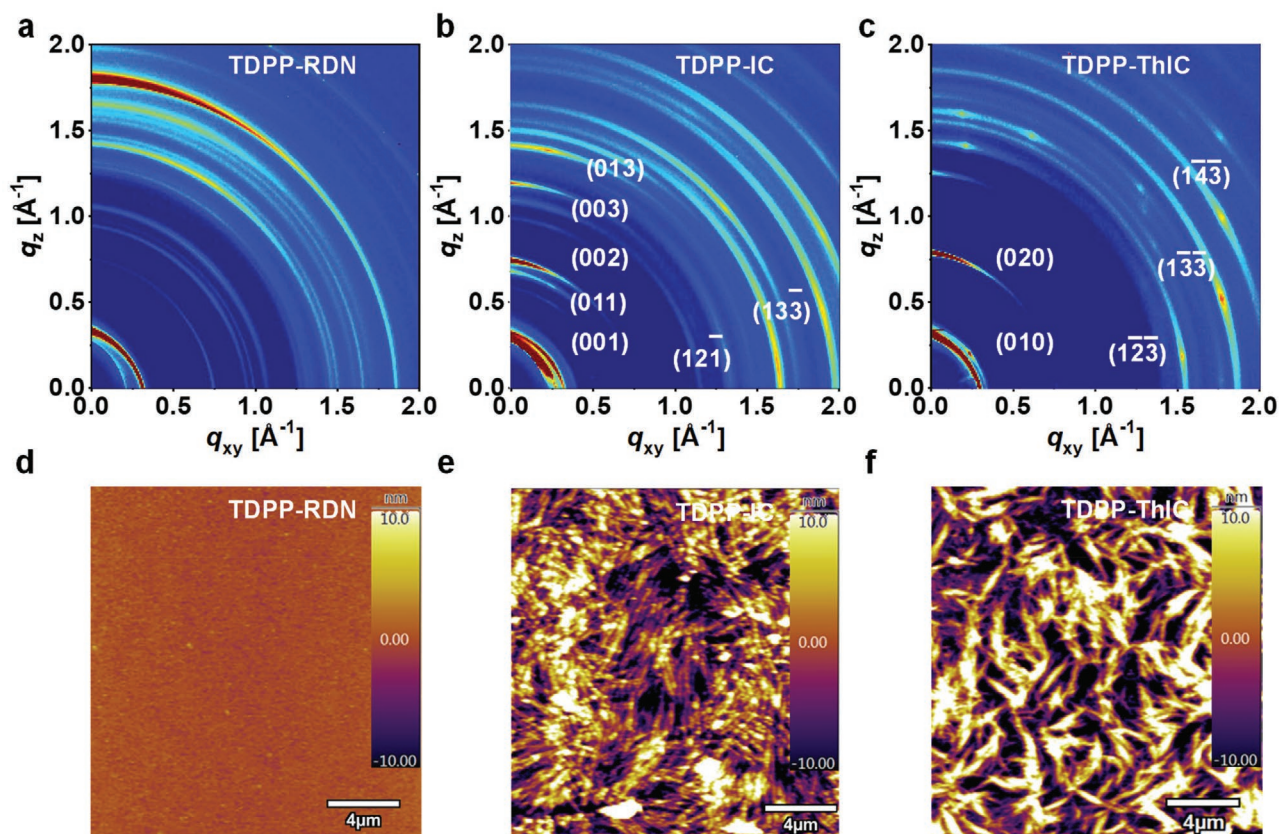


Figure 3. GIWAXS patterns and AFM height images of a,d) TDPP-RDN film, b,e) TDPP-IC film, and c,f) TDPP-ThIC film prepared by spin-coating their CB solutions.

packings of TDPP-IC and TDPP-ThIC are very similar to their single crystal structures because most of diffraction peaks from GIWAXS are consistent with those simulated from their single crystal data (Figure S7, Supporting Information).^[60–63] The detailed q value, d -spacing, and 2θ of each diffraction peaks are listed in Table S2, Supporting Information. Among all the diffractions, the (13-3) and (1-3-3) diffraction peaks from the films of TDPP-IC and TDPP-ThIC represent the diffractions from their respective π -planes. Both TDPP-IC and TDPP-ThIC show an “edge-on” packing on a substrate with the tilt angles between the π -planes and the substrate of 78.35° for TDPP-IC and 67.93° for TDPP-ThIC (Figure 4a). Besides, the π - π stacking distances measured from the thin films are 3.52 \AA for TDPP-IC and 3.50 \AA for TDPP-ThIC, which are very close to their intracolumn π - π stacking distances in the single crystal structures. Considering the smaller intercolumn π - π stacking distances formed by the end functional groups, the closer intracolumn and intercolumn packing in TDPP-ThIC might explain its higher electron mobility.^[64] Due to the lack of the single crystal structure of TDPP-RDN, its molecular packing and exact arrangement in thin film are unknown. However, from the 2D GIWAXS, the film of TDPP-RDN shows obvious diffraction peaks at $q_z = 0.41$ and 1.59 \AA^{-1} in out-of-plane (OOP, q_z) direction, suggesting that TDPP-RDN shows a disordered molecular packing with both face-on, edge-on, and other orientations in the thin film, which might be responsible for its low electron mobility.

From the AFM height images, TDPP-RDN film shows a uniform and smooth surface with a low root-mean-square (RMS) roughness of 0.87 nm (Figure 3d). In contrast, the films of TDPP-IC and TDPP-ThIC show rough surfaces with the RMS roughness of 8.38 and 8.98 nm , respectively (Figures 3e and 3f). The larger RMS values imply that TDPP-IC and TDPP-ThIC tend to form more crystallized films compared to TDPP-RDN. The films of TDPP-IC and TDPP-ThIC both display fibrous microstructures, suggesting that they tend to grow in a 1D fashion. Based on the GIWAXS and AFM results, we can conclude that the molecular interactions can be well-tuned by the different end functional groups, and ThIC provides stronger intercolumn interactions, leading to enhanced crystallinity and improved charge carrier mobility in thin film.

2.4. Charge Transport and Solid-State Microstructures of Doped Films

N-DMBI was chosen as the n-dopant because of its good air stability and strong n-doping capability.^[65,66] The doping levels of three molecules in the solution were evaluated by absorption spectroscopy. As increasing the *N*-DMBI/molecule ratio from 0% to 200 mol%, the absorption spectrum of TDPP-RDN only shows a little change in the intensity (Figure 5a), whereas TDPP-IC and TDPP-ThIC show obviously decreased absorption intensity at Band I (550–1000 nm) region and an increased

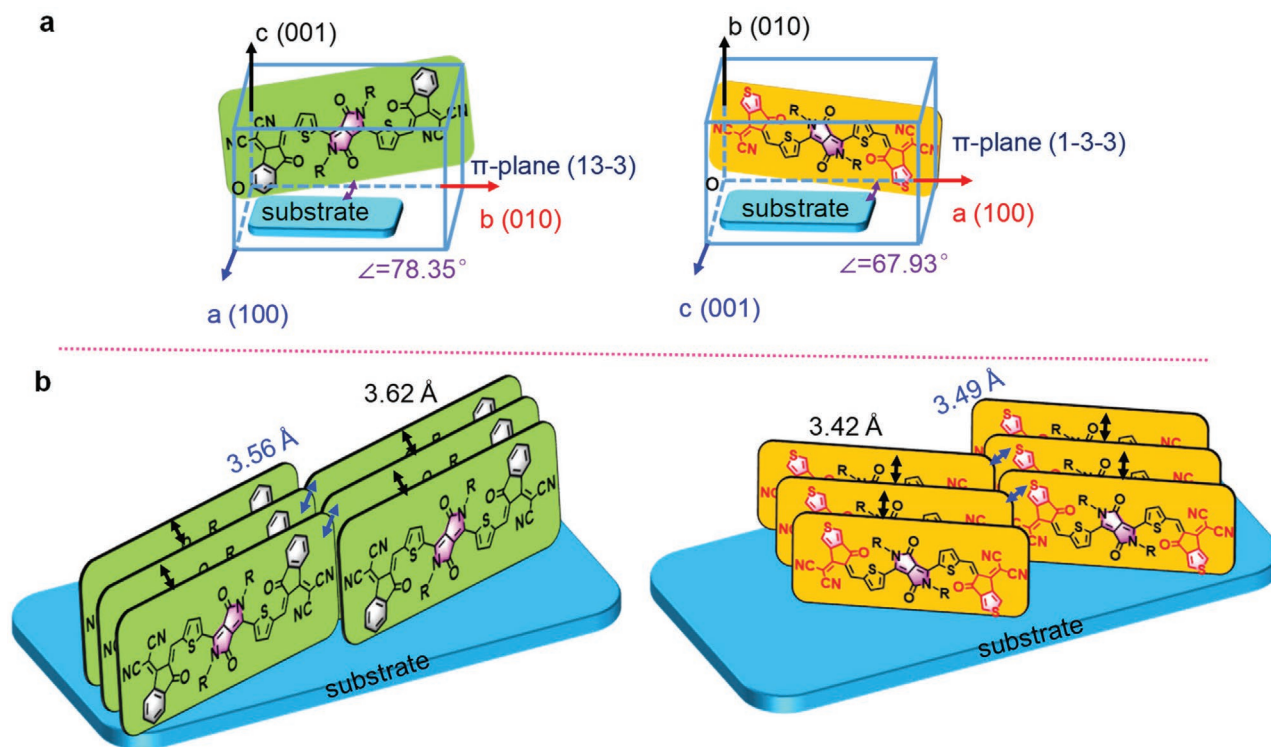


Figure 4. a) The molecular orientations of TDPP-IC and TDPP-ThIC obtained by comparing their GIWAXS and single crystal data. The tilt angles between their respective π -planes and the substrate are marked. b) Their molecular packings and orientations in thin films. The intracolumn (black) and intercolumn (blue) π - π stacking distances come from their single crystal structures.

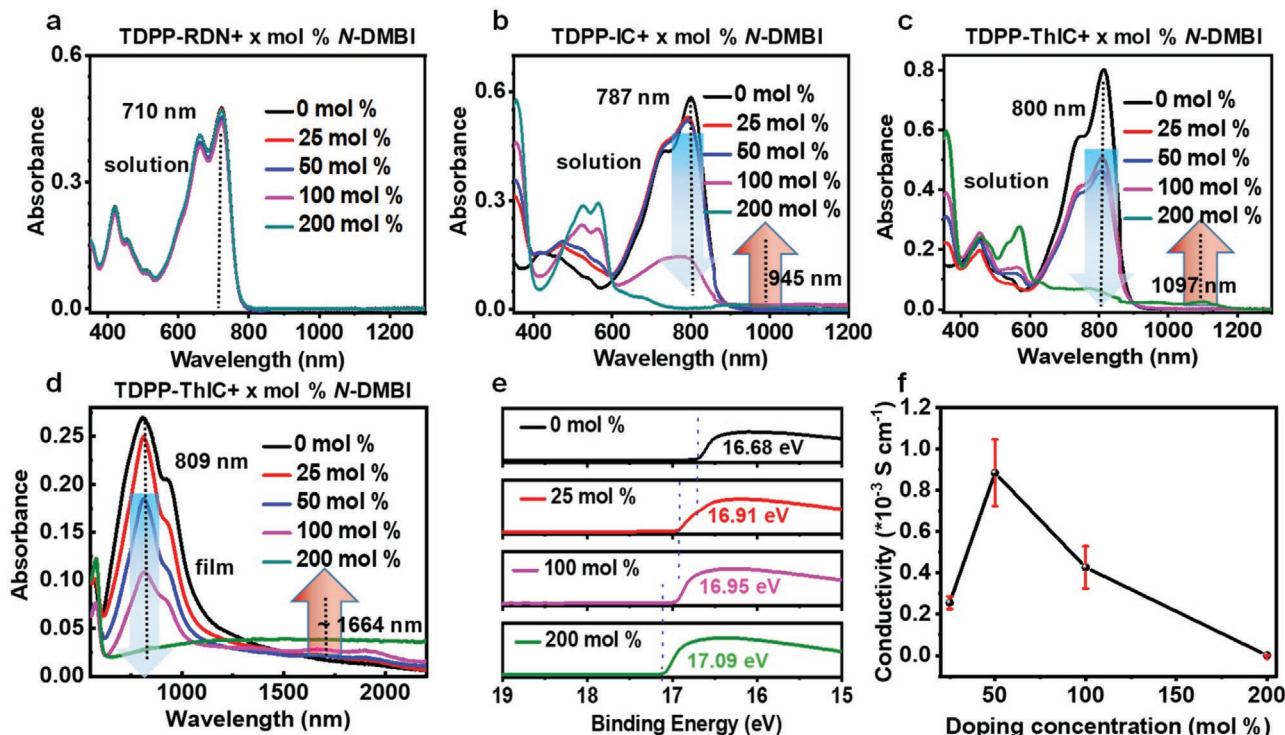


Figure 5. The pristine and the doped UV-Vis-NIR absorption spectra of a) TDPP-RDN, b) TDPP-IC, and c) TDPP-ThIC in CB solutions with various *N*-DMBI mole ratios. d) The absorption spectra of the pristine and the doped TDPP-ThIC films. e) The UPS binding energy of the pristine and the doped TDPP-ThIC films with the different *N*-DMBI mole ratios. The locations of secondary electron cut-off (SECO) are marked with dashed lines. f) Electrical conductivity of the doped TDPP-ThIC films with different concentrations of *N*-DMBI.

new absorption band at NIR region (>900 nm). Compared to TDPP-IC, the absorption spectrum change is more pronounced for TDPP-ThIC, especially at low doping concentrations (0 to 25 mol%). The new NIR band can be attributed to the polaron or bipolaron absorptions after doping.^[41,67,68] These results indicate that compared to TDPP-RDN, TDPP-IC, and TDPP-ThIC can be effectively doped with *N*-DMBI in solution, and at low dopant concentrations, TDPP-ThIC is more readily doped. These results are expected because TDPP-RDN, TDPP-IC, and TDPP-ThIC have gradually decreased LUMO energy levels with increased electron-withdrawing ability.

In solid state, the absorption intensity at ≈1664 nm of the doped TDPP-ThIC films, which can be attributed to the polaron or bipolaron absorption, gradually promotes as increasing the *N*-DMBI/molecule ratio (Figure 5d). The Band I absorption disappeared when 200 mol% *N*-DMBI was added, suggesting a complete reduction of the neutral molecules. In contrast, TDPP-RDN films show an incomplete reduction at this doping concentration (Figure S8, Supporting Information). The decline of the main absorption peaks and generation of the polaron or bipolaron peaks in solid state are more obvious than in solution, implying doping can occur to TDPP-RDN in solid state. Ultraviolet photoelectron spectroscopy (UPS) and X-ray photoelectron spectroscopy (XPS) were used to gain more insight into the doping process. In Figure 5e, the secondary electron cut-off (SECO) of the TDPP-ThIC films gradually shifts from 16.68 to 17.09 eV as increasing the *N*-DMBI mole ratio, suggesting the Fermi level (E_F) moves toward the LUMO energy level in the doped films. A similar situation was also found in X-ray photoelectron spectroscopy (XPS) spectra. After doping with *N*-DMBI, the N (1s) peak of cyano groups at 399.10 eV shows an obvious shift (Figure S9, Supporting Information). The new generated N (1s) peak at 401.41 eV in the doped films is attributed to the formation of *N*-DMBI⁺. All the results imply that TDPP-ThIC film can be effectively doped with *N*-DMBI. The electrical conductivities of doped TDPP-RDN, TDPP-IC, and TDPP-ThIC films were measured as a function of the *N*-DMBI/molecule ratio (Figure 5f and Figure S10, Supporting Information). Among them, TDPP-ThIC shows the highest electrical conductivity of $9 \times 10^{-4} \text{ S cm}^{-1}$ when doped with 50 mol% *N*-DMBI. This value is higher than those of TDPP-RDN ($2 \times 10^{-5} \text{ S cm}^{-1}$) and TDPP-IC ($8 \times 10^{-4} \text{ S cm}^{-1}$) at their optimal doping concentrations. Besides, doping stability was also measured for TDPP-ThIC (Figure S11, Supporting Information). TDPP-ThIC shows good stability in a nitrogen glovebox with only 15% decay from its initial electrical conductivity after 9 h storage; whereas at 120 °C, the electrical conductivity decreased significantly, suggesting that the doped small molecules might not be thermally stable at higher temperatures. On the other hand, since TDPP-ThIC films have high electron mobilities over $0.7 \text{ cm}^2 \text{ s}^{-1} \text{ V}^{-1}$ and can be effectively doped, we expect the molecule could show a high n-doped electrical conductivity.^[31] However, the highest electrical conductivity of doped TDPP-ThIC films is only $9 \times 10^{-4} \text{ S cm}^{-1}$, which is much lower than the small molecules with similar electron mobilities.^[33,37,69]

To understand the reasons for the low electrical conductivity, GIWAXS and AFM were used for the doped TDPP-ThIC films. From Figures 6a–e, as increasing the *N*-DMBI mole ratio, the diffraction peaks become weaker and broader. Accordingly,

the coherence lengths of the (010)/(020) peaks decrease from 193.5/319.4 to 179.6/225.9 Å with the ratio of *N*-DMBI/molecule from 0 to 100 mol%, indicating gradually weakened crystallinity in the doped films (Figure S12 and Table S3, Supporting Information). When 200 mol% *N*-DMBI is added, the diffraction signals almost disappear. The results indicate that the molecular packing of TDPP-ThIC in the doped films is gradually damaged as increasing the *N*-DMBI mole ratio. The *d*-spacings of (020), (1-2-3), (1-3-3), and (1-4-3) diffraction peaks in the doped TDPP-ThIC films were extracted. The *d*-spacings of these diffraction peaks shift to larger values as increasing the *N*-DMBI mole ratio (Figure S13, Supporting Information). Particularly, (1-4-3) (intercolumn packing) and (020) (lamellar packing) diffraction peaks show more obvious shifts, suggesting that the *N*-DMBI⁺ might exist in the intercolumn and alkyl side chain regions (Figure 6k). These results are expected because the side-chain packing and intercolumn packing are weaker than the intracolumn π - π stacking ((1-3-3) direction). Therefore, after n-doping, the intercolumn charge transport pathways are more strongly affected than the intracolumn charge transport pathways, and all the charge transport pathways are gradually damaged as increasing the dopant mole ratio. AFM height images show that the RMS roughness gradually reduces with 8.98 nm for 0 mol%, 4.03 nm for 25 mol%, and 1.95 nm for 50 mol%, indicating that the *N*-DMBI reduced the molecular crystallinity, which is consistent with the GIWAXS results (Figure 6f–j). When adding more *N*-DMBI, the films show larger RMS values of 11.63 nm for 100 mol% and 25.50 nm for 200 mol%, suggesting that *N*-DMBI/TDPP-ThIC might form phase separations at these higher dopant ratios.

Besides, the charge transport property of the lightly doped TDPP-ThIC films was also measured using a FET device (Figure S14, Supporting Information). With the doping concentrations increasing (2.5, 5, and 75 mol%), the electron mobilities of the doped TDPP-ThIC films show sharply decrease from original $0.69 \text{ cm}^2 \text{ V}^{-1} \text{ s}^{-1}$ to 0.08, 0.06, and $0.02 \text{ cm}^2 \text{ V}^{-1} \text{ s}^{-1}$, respectively. The on/off ratio also decreased significantly even at a low doping concentration of 2.5 mol%. These results indicate that *N*-DMBI can efficiently dope with TDPP-ThIC at low doping concentrations. In conjugated polymers, we often observe increased mobility after lightly doping due to the trap-filling effect.^[70,71] However, for TDPP-ThIC, the mobility sharply decreases after lightly doping. These results further support that the molecular packing and charge transport pathways are largely damaged even at low dopant concentrations. Based on the above results, the change of electrical conductivity as increasing the dopant ratio can be understood. At low dopant/TDPP-ThIC ratios, TDPP-ThIC can be effectively doped, and free electrons are generated, leading to a relatively higher electrical conductivity ($9 \times 10^{-4} \text{ S cm}^{-1}$) at 50 mol% *N*-DMBI. However, because the charge transport pathways are damaged and molecular crystallinity gradually reduces, the electrical conductivity remains low compared with other high conductivities' small molecules or conjugated polymers. It seems like that intercolumn packing is more critical because intercolumn interactions are weaker, and more easily damaged by enthetic dopants than intracolumn interactions. At higher dopant/TDPP-ThIC ratios (>50 mol%), the electrical conductivities sharply decrease, which is largely due to

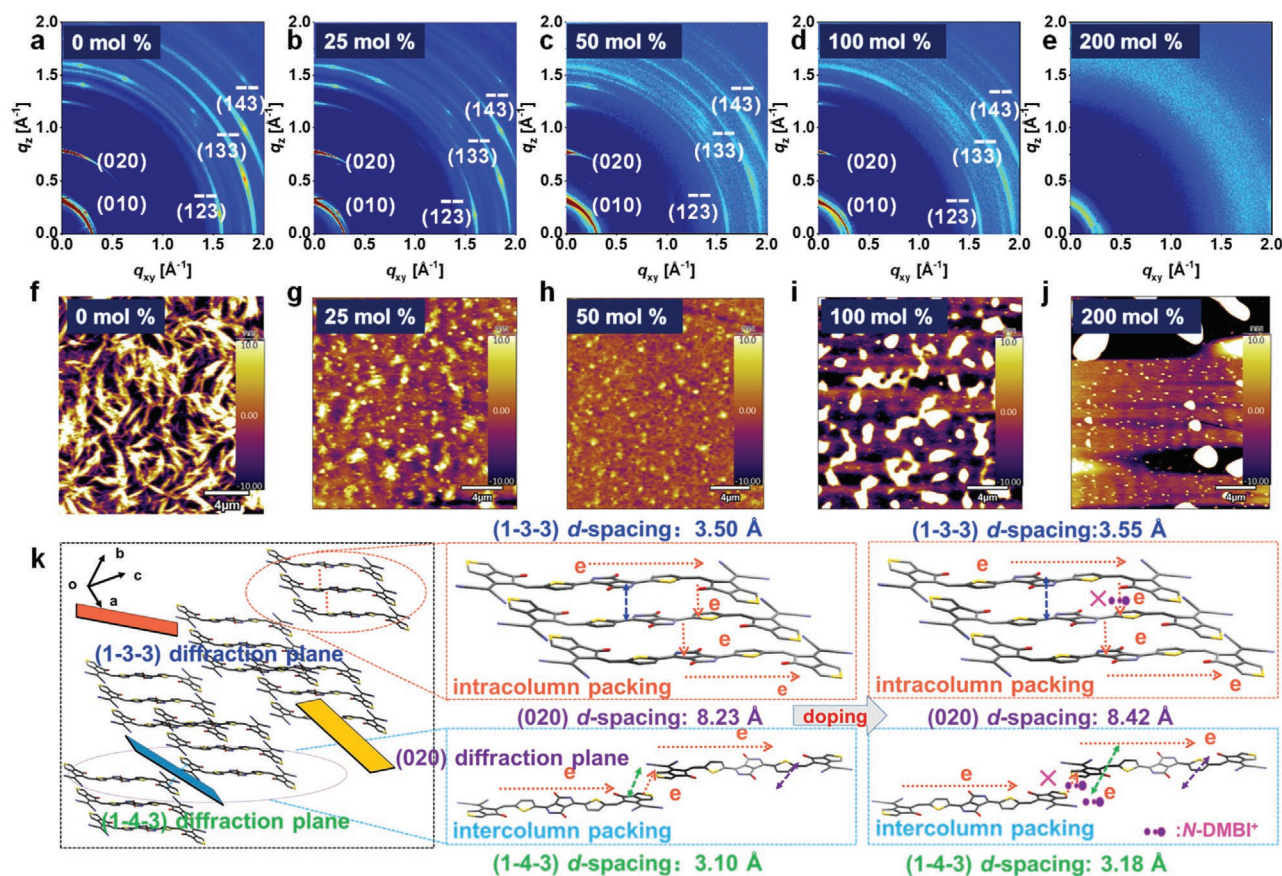


Figure 6. The GIWAXS patterns (a–e) and AFM height images (f–j) of the pristine and the doped films with the different *N*-DMBI mole ratios. k) The changes of the (020), (1-3-3), and (1-4-3) *d*-spacings after doping. (1-3-3) diffraction plane in the illustration indexes the π - π stacking direction, (020) diffraction plane indexes the side-chain packing direction, and (1-4-3) diffraction plane mainly indexes intercolumn packing direction.

the dopant-small molecule phase separation and the further damage of the molecular packing and crystallinity. Our results imply that high intrinsic charge carrier mobility and low LUMO energy level cannot guarantee high *n*-doped electrical conductivity in small molecules because the film crystallinity could be largely reduced, and charge transport pathways might be significantly damaged at both the molecular packing scale and the crystal grain scale.

3. Conclusion

In summary, we have synthesized three small molecules to explore the low electrical conductivity issues for small molecule OTE materials. The three molecules have similar backbones but with different end functional groups. Benefiting from its planar heteroatom-containing end group, TDPP-ThIC shows outstanding electron mobilities of up to $0.77 \text{ cm}^2 \text{ V}^{-1} \text{ s}^{-1}$ and can be effectively doped by *N*-DMBI. However, its electrical conductivity is comparatively low. Using multiple characterizations, we find that the molecular packing of TDPP-ThIC is easily distorted by the *n*-dopants, which damages the charge transport pathways and thereby results in low electrical conductivity. Our results suggest that to address the low electrical conductivity issue in *n*-doped small molecule semiconductors, it is

critical to strengthen the intermolecular interactions (especially for the weak intercolumn interactions here), avoid dopant-induced structural disorder (leading to low film crystallinity), and enhance the dopant-molecule miscibility.

Supporting Information

Supporting Information is available from the Wiley Online Library or from the author.

Acknowledgements

G.-Y.G. and J.-T.L. contributed equally to this work. This work was financially supported by grants from the Natural Science Foundation of China (No. 21971014, 21672023) and the National Key Research and Development Program of China (2018YFA0901800). J.-L.W. was supported by the BIT Teli Young Fellow Recruitment Program. T.L. thanks the support from National Natural Science Foundation of China (22075001). Part of the computational work is supported by High-performance Computing Platform of Peking University. The authors thank Prof. Jian Pei (Peking University) for helpful discussions. G.-Y.G. thank Dr. Rui Zhu and Asif Mahmood (Beijing Institute of Technology) for density functional theory calculations. G.-Y.G. thanks Dr. Hai-Rong Huo and Jin-Mei Ma (Beijing Institute of Technology) for the synthesis of ThIC. G.-Y.G. thanks Yue Guo and Junfang Wang for the

help on the synthesis of precursors. The authors thank the Analysis & Testing Center, Beijing Institute of Technology for the NMR and TGA experiments. The authors thank Prof. Hai-Jun Fan, Prof. Xiaozhang Zhu, and Dr. Yongjie Chen (Chinese Academy of Sciences) for the help on single-crystal measurements. The authors are grateful for having been able to use the beamline BL14B1 (Shanghai Synchrotron Radiation Facility) for 2D GIWAXS experiments. The authors thank Dr. Kai-Kai Liu (Peking University) and Dr. Ze-Fan Yao (Peking University) for crystallographic and 2D GIWAXS analysis. The authors thank Prof. Jian Pei and Prof. Jie-Yu Wang (Peking University) for the help on UV-Vis-NIR absorption spectra and AFM measurements. G.-Y.G. thanks Dr. Lu Yan and Hai-Rui Bai (Beijing Institute of Technology) for the help on 2D GIWAXS measurements in Shanghai Synchrotron Radiation Facility.

Conflict of Interest

The authors declare no conflict of interest.

Data Availability Statement

The data that support the findings of this study are openly available in The Cambridge Crystallographic Data Centre (CCDC) via www.ccdc.cam.ac.uk/data_request/cif with the No.s of 2096378 and 2083909.

Keywords

charge transport, electrical conductivity, molecular packing, N-doping, organic semiconductors

Received: August 19, 2021
Revised: September 30, 2021
Published online:

- [1] W. Zhao, J. Ding, Y. Zou, C.-a. Di, D. Zhu, *Chem. Soc. Rev.* **2020**, 49, 7210.
- [2] M. Lindorf, K. A. Mazzio, J. Pflaum, K. Nielsch, W. Brütting, M. Albrecht, *J. Mater. Chem. A* **2020**, 8, 7495.
- [3] G. Zuo, H. Abdalla, M. Kemerink, *Adv. Electron. Mater.* **2019**, 5, 1800821.
- [4] S. Griggs, A. Marks, H. Bristow, I. McCulloch, *J. Mater. Chem. C* **2021**, 9, 8099.
- [5] T. L. D. Tam, J. Xu, *J. Mater. Chem. A* **2021**, 9, 5149.
- [6] G. H. Kim, L. Shao, K. Zhang, K. P. Pipe, *Nat. Mater.* **2013**, 12, 719.
- [7] H. J. Lee, G. Anoop, H. J. Lee, C. Kim, J.-W. Park, J. Choi, H. Kim, Y.-J. Kim, E. Lee, S.-G. Lee, Y.-M. Kim, J.-H. Lee, J. Y. Jo, *Energy Environ. Sci.* **2016**, 9, 2806.
- [8] Y. Sun, C.-a. Di, W. Xu, D. Zhu, *Adv. Electron. Mater.* **2019**, 5, 1800825.
- [9] J.-T. Li, T. Lei, *Chem. - Asian J.* **2021**, 16, 1508.
- [10] C. Zhang, X. Zhu, *Adv. Funct. Mater.* **2020**, 30, 2000765.
- [11] H. Sun, X. Guo, A. Facchetti, *Chem* **2020**, 6, 1310.
- [12] Y. Lu, J.-Y. Wang, J. Pei, *Chem. Mater.* **2019**, 31, 6412.
- [13] J. Han, C. Ganley, Q. Hu, X. Zhao, P. Clancy, T. P. Russell, H. E. Katz, *Adv. Funct. Mater.* **2021**, 31, 2010567.
- [14] C.-Y. Yang, M.-A. Stoeckel, T.-P. Ruoko, H.-Y. Wu, X. Liu, N. B. Kolhe, Z. Wu, Y. Püttison, C. Musumeci, M. Massetti, H. Sun, K. Xu, D. Tu, W. M. Chen, H. Y. Woo, M. Fahlman, S. A. Jenekhe, M. Berggren, S. Fabiano, *Nat. Commun.* **2021**, 12, 2354.
- [15] S. E. Yoon, J. Park, J. E. Kwon, S. Y. Lee, J. M. Han, C. Y. Go, S. Choi, K. C. Kim, H. Seo, J. H. Kim, B.-G. Kim, *Adv. Mater.* **2020**, 32, 2005129.
- [16] H. Chen, M. Moser, S. Wang, C. Jellett, K. Thorley, G. T. Harrison, X. Jiao, M. Xiao, B. Purushothaman, M. Alsufyani, H. Bristow, S. De Wolf, N. Gasparini, A. Wadsworth, C. R. McNeill, H. Sirringhaus, S. Fabiano, I. McCulloch, *J. Am. Chem. Soc.* **2021**, 143, 260.
- [17] M. Xiong, X. Yan, J.-T. Li, S. Zhang, Z. Cao, N. Prine, Y. Lu, J.-Y. Wang, X. Gu, T. Lei, *Angew. Chem., Int. Ed.* **2021**, 60, 8189.
- [18] Y. Lu, Z.-D. Yu, Y. Liu, Y.-F. Ding, C.-Y. Yang, Z.-F. Yao, Z.-Y. Wang, H.-Y. You, X.-F. Cheng, B. Tang, J.-Y. Wang, J. Pei, *J. Am. Chem. Soc.* **2020**, 142, 15340.
- [19] X. Yan, M. Xiong, J.-T. Li, S. Zhang, Z. Ahmad, Y. Lu, Z.-Y. Wang, Z.-F. Yao, J.-Y. Wang, X. Gu, T. Lei, *J. Am. Chem. Soc.* **2019**, 141, 20215.
- [20] K. Feng, H. Guo, J. Wang, Y. Shi, Z. Wu, M. Su, X. Zhang, J. H. Son, H. Y. Woo, X. Guo, *J. Am. Chem. Soc.* **2021**, 143, 1539.
- [21] Q. Jiang, H. Sun, D. Zhao, F. Zhang, D. Hu, F. Jiao, L. Qin, V. Linseis, S. Fabiano, X. Crispin, Y. Ma, Y. Cao, *Adv. Mater.* **2020**, 32, 2002752.
- [22] J. Liu, G. Ye, H. G. O. Potgieser, M. Koopmans, S. Sami, M. I. Nugraha, D. R. Villalva, H. Sun, J. Dong, X. Yang, X. Qiu, C. Yao, G. Portale, S. Fabiano, T. D. Anthopoulos, D. Baran, R. W. A. Havenith, R. C. Chiechi, L. J. A. Koster, *Adv. Mater.* **2021**, 33, 2006694.
- [23] C. Dong, S. Deng, B. Meng, J. Liu, L. Wang, *Angew. Chem., Int. Ed.* **2021**, 60, 16184.
- [24] H. Wei, P.-A. Chen, J. Guo, Y. Liu, X. Qiu, H. Chen, Z. Zeng, T.-Q. Nguyen, Y. Hu, *Adv. Funct. Mater.* **2021**, 31, 2102768.
- [25] Y. Wang, K. Takimiya, *Adv. Mater.* **2020**, 32, 2002060.
- [26] O. Bardagot, P. Kubik, T. Marszalek, P. Veyre, A. A. Medjahed, M. Sandroni, B. Grévin, S. Pouget, T. Nunes Domschke, A. Carella, S. Gambarelli, W. Pisula, R. Demadrille, *Adv. Funct. Mater.* **2020**, 30, 2000449.
- [27] L. Xiang, L. Liu, F. Zhang, C.-a. Di, D. Zhu, *Adv. Funct. Mater.* **2021**, 31, 2102149.
- [28] Y. Lu, Z.-D. Yu, H.-I. Un, Z.-F. Yao, H.-Y. You, W. Jin, L. Li, Z.-Y. Wang, B.-W. Dong, S. Barlow, E. Longhi, C.-a. Di, D. Zhu, J.-Y. Wang, C. Silva, S. R. Marder, J. Pei, *Adv. Mater.* **2021**, 33, 2005946.
- [29] J. Liu, G. Ye, B. v. d. Zee, J. Dong, X. Qiu, Y. Liu, G. Portale, R. C. Chiechi, L. J. A. Koster, *Adv. Mater.* **2018**, 30, 1804290.
- [30] C. Yang, Q. An, H.-R. Bai, H.-F. Zhi, H. S. Ryu, A. Mahmood, X. Zhao, S. Zhang, H. Y. Woo, J.-L. Wang, *Angew. Chem., Int. Ed.* **2021**, 60, 19241.
- [31] F. Zhang, C.-a. Di, *Chem. Mater.* **2020**, 32, 2688.
- [32] J.-L. Wang, K.-K. Liu, L. Hong, G.-Y. Ge, C. Zhang, J. Hou, *ACS Energy Lett.* **2018**, 3, 2967.
- [33] D. Yuan, D. Huang, S. M. Rivero, A. Carreras, C. Zhang, Y. Zou, X. Jiao, C. R. McNeill, X. Zhu, C.-a. Di, D. Zhu, D. Casanova, J. Casado, *Chem* **2019**, 5, 964.
- [34] D. Huang, C. Wang, Y. Zou, X. Shen, Y. Zang, H. Shen, X. Gao, Y. Yi, W. Xu, C.-a. Di, D. Zhu, *Angew. Chem., Int. Ed.* **2016**, 55, 10672.
- [35] K. Yang, X. Zhang, A. Harbuzaru, L. Wang, Y. Wang, C. Koh, H. Guo, Y. Shi, J. Chen, H. Sun, K. Feng, M. C. Ruiz Delgado, H. Y. Woo, R. P. Ortiz, X. Guo, *J. Am. Chem. Soc.* **2020**, 142, 4329.
- [36] D. Yuan, Y. Guo, Y. Zeng, Q. Fan, J. Wang, Y. Yi, X. Zhu, *Angew. Chem., Int. Ed.* **2019**, 58, 4958.
- [37] D. Huang, H. Yao, Y. Cui, Y. Zou, F. Zhang, C. Wang, H. Shen, W. Jin, J. Zhu, Y. Diao, W. Xu, C.-a. Di, D. Zhu, *J. Am. Chem. Soc.* **2017**, 139, 13013.
- [38] J. Liu, B. van der Zee, R. Alessandri, S. Sami, J. Dong, M. I. Nugraha, A. J. Barker, S. Rouseva, L. Qiu, X. Qiu, N. Klasen, R. C. Chiechi, D. Baran, M. Caironi, T. D. Anthopoulos, G. Portale, R. W. A. Havenith, S. J. Marrink, J. C. Hummelen, L. J. A. Koster, *Nat. Commun.* **2020**, 11, 5694.
- [39] D. Yuan, W. Liu, X. Zhu, *Chem* **2021**, 7, 333.
- [40] Y. Min, C. Dong, H. Tian, J. Liu, L. Wang, *ACS Appl. Mater. Interfaces* **2021**, 13, 33321.

- [41] J. Liu, B. Van der Zee, D. R. Villava, G. Ye, S. Kahmann, M. Kamperman, J. Dong, L. Qiu, G. Portale, M. A. Loi, J. C. Hummelen, R. C. Chiechi, D. Baran, L. J. A. Koster, *ACS Appl. Mater. Interfaces* **2021**, *13*, 29858.
- [42] G. Krauss, F. Meichsner, A. Hochgesang, J. Mohanraj, S. Salehi, P. Schmode, M. Thelakkat, *Adv. Funct. Mater.* **2021**, *31*, 2010048.
- [43] Y. Zhou, W. Zhang, G. Yu, *Chem. Sci.* **2021**, *12*, 6844.
- [44] W. Jiang, Z. Liu, D. Zhu, W. Zheng, L. Chen, X. Zhang, G. Zhang, Y. Yi, L. Jiang, D. Zhang, *Angew. Chem., Int. Ed.* **2021**, *60*, 10700.
- [45] H. Li, J. Song, J. Xiao, L. Wu, H. E. Katz, L. Chen, *Adv. Funct. Mater.* **2020**, *30*, 2004378.
- [46] S.-L. Wu, Y.-F. Huang, C.-T. Hsieh, B.-H. Lai, P.-S. Tseng, J.-T. Ou, S.-T. Liao, S.-Y. Chou, K.-Y. Wu, C.-L. Wang, *ACS Appl. Mater. Interfaces* **2017**, *9*, 14967.
- [47] Q. Zhou, Y. Jiang, T. Du, Z. Wang, Z. Liang, Y. Han, Y. Deng, H. Tian, Y. Geng, *J. Mater. Chem. C* **2019**, *7*, 13939.
- [48] H. S. Ryu, M. J. Kim, Y. W. Lee, S.-H. Lee, T. J. Shin, J. H. Cho, H. Y. Woo, *ACS Appl. Mater. Interfaces* **2019**, *11*, 47170.
- [49] L. Wang, Q. An, L. Yan, H.-R. Bai, M. Jiang, A. Mahmood, C. Yang, H. Zhi, J.-L. Wang, *Energy Environ. Sci.* **2021**, <https://doi.org/10.1039/D1EE01832A>.
- [50] R. Ma, T. Liu, Z. Luo, K. Gao, K. Chen, G. Zhang, W. Gao, Y. Xiao, T.-K. Lau, Q. Fan, Y. Chen, L.-K. Ma, H. Sun, G. Cai, T. Yang, X. Lu, E. Wang, C. Yang, A. K. Y. Jen, H. Yan, *ACS Energy Lett.* **2020**, *5*, 2711.
- [51] Z. Luo, T. Liu, H. Yan, Y. Zou, C. Yang, *Adv. Funct. Mater.* **2020**, *30*, 2004477.
- [52] J. Yuan, T. Huang, P. Cheng, Y. Zou, H. Zhang, J. L. Yang, S.-Y. Chang, Z. Zhang, W. Huang, R. Wang, D. Meng, F. Gao, Y. Yang, *Nat. Commun.* **2019**, *10*, 570.
- [53] W. Hong, B. Sun, H. Aziz, W.-T. Park, Y.-Y. Noh, Y. Li, *Chem. Commun.* **2012**, *48*, 8413.
- [54] H. Huang, L. Yang, A. Facchetti, T. J. Marks, *Chem. Rev.* **2017**, *117*, 10291.
- [55] Y. Li, J. Zhang, S. Liu, C. Zhang, C. Chuah, Y. Tang, R. T. K. Kwok, J. W. Y. Lam, H. Ou, D. Ding, B. Z. Tang, *Adv. Funct. Mater.* **2021**, *31*, 2102213.
- [56] N. J. Hestand, F. C. Spano, *Chem. Rev.* **2018**, *118*, 7069.
- [57] T. Sarkar, S. A. Schneider, G. Ankonina, A. D. Hendsbee, Y. Li, M. F. Toney, G. L. Frey, *Chem. Mater.* **2020**, *32*, 7338.
- [58] Z.-F. Yao, Y.-Q. Zheng, Q.-Y. Li, T. Lei, S. Zhang, L. Zou, H.-Y. Liu, J.-H. Dou, Y. Lu, J.-Y. Wang, X. Gu, J. Pei, *Adv. Mater.* **2019**, *31*, 1806747.
- [59] Y. Xu, R. Gwoziecki, I. Chartier, R. Coppard, F. Balestra, G. Ghibaudo, *Appl. Phys. Lett.* **2010**, *97*, 063302.
- [60] G.-Y. Ge, W. Xiong, K.-K. Liu, H. S. Ryu, S.-S. Wan, B. Liu, A. Mahmood, H.-R. Bai, J.-F. Wang, Z. Wang, H. Y. Woo, Y. Sun, J.-L. Wang, *J. Mater. Chem. C* **2021**, *9*, 1923.
- [61] S. E. Fritz, S. M. Martin, C. D. Frisbie, M. D. Ward, M. F. Toney, *J. Am. Chem. Soc.* **2004**, *126*, 4084.
- [62] S. C. B. Mannsfeld, M. L. Tang, Z. Bao, *Adv. Mater.* **2011**, *23*, 127.
- [63] S. Dai, J. Zhou, S. Chandrabose, Y. Shi, G. Han, K. Chen, J. Xin, K. Liu, Z. Chen, Z. Xie, W. Ma, Y. Yi, L. Jiang, J. M. Hodgkiss, X. Zhan, *Adv. Mater.* **2020**, *32*, 2000645.
- [64] G. Giri, E. Verploegen, S. C. B. Mannsfeld, S. Atahan-Evrenk, D. H. Kim, S. Y. Lee, H. A. Becerril, A. Aspuru-Guzik, M. F. Toney, Z. Bao, *Nature* **2011**, *480*, 504.
- [65] P. Wei, T. Menke, B. D. Naab, K. Leo, M. Riede, Z. Bao, *J. Am. Chem. Soc.* **2012**, *134*, 3999.
- [66] M. Alsufyani, R. K. Hallani, S. Wang, M. Xiao, X. Ji, B. D. Paulsen, K. Xu, H. Bristow, H. Chen, X. Chen, H. Siringhaus, J. Rivnay, S. Fabiano, I. McCulloch, *J. Mater. Chem. C* **2020**, *8*, 15150.
- [67] S. Wang, T.-P. Ruoko, G. Wang, S. Riera-Galindo, S. Hultmark, Y. Puttison, F. Moro, H. Yan, W. M. Chen, M. Berggren, C. Müller, S. Fabiano, *ACS Appl. Mater. Interfaces* **2020**, *12*, 53003.
- [68] Y. Zeng, W. Zheng, Y. Guo, G. Han, Y. Yi, *J. Mater. Chem. A* **2020**, *8*, 8323.
- [69] D. Yuan, D. Huang, C. Zhang, Y. Zou, C.-a. Di, X. Zhu, D. Zhu, *ACS Appl. Mater. Interfaces* **2017**, *9*, 28795.
- [70] H. Shimotani, G. Diguët, Y. Iwasa, *Appl. Phys. Lett.* **2005**, *86*, 022104.
- [71] C.-Y. Yang, W.-L. Jin, J. Wang, Y.-F. Ding, S. Nong, K. Shi, Y. Lu, Y.-Z. Dai, F.-D. Zhuang, T. Lei, C.-A. Di, D. Zhu, J.-Y. Wang, J. Pei, *Adv. Mater.* **2018**, *30*, 1802850.